ISSN 1069-3513, Izvestiya, Physics of the Solid Earth, 2014, Vol. 50, No. 2, pp. 177–191. © Pleiades Publishing, Ltd., 2014.
Original Russian Text © V.O. Mikhailov, I. Panet, M. Hayn, E.P. Timoshkina, S. Bonvalot, V. Lyakhovsky, M. Diament, O. de Viron, 2014, published in Fizika Zemli, 2014, No. 2, pp. 187–198.

Comparative Study of Temporal Variations in the Earth's Gravity Field Using GRACE Gravity Models in the Regions of Three Recent Giant Earthquakes

V. O. Mikhailov[a, b], I. Panet[c], M. Hayn[b], E. P. Timoshkina[a, b], S. Bonvalot[d], V. Lyakhovsky[e], M. Diament[b], and O. de Viron[b]

[a] *Schmidt Institute of Physics of the Earth, Russian Academy of Sciences, ul. Bol'shaya Gruzinskaya 10, Moscow, 123995 Russia*

[b] *Université Paris Diderot, Sorbonne Paris Cité, Institut de Physique du Globe de Paris, Paris, France*

[c] *Institut National de l'Information Geographique et Forestiere, Laboratoire LAREG, Universite Paris Diderot; Paris Cedex 13, France*

[d] *Institut de Recherche pour le Développement (IRD), Bureau Gravimétrique International (BGI)—GET (UMR5563 CNRS/IRD/UT3), Toulouse, France*

e-mail: sylvain.bonvalot@ird.fr

[e] *Geological Survey of Israel, Jerusalem, 95501 Israel*

e-mail: vladi@geos.gsi.gov.il

Received June 15, 2013; in final form, October 9, 2013

Abstract—Comparative analysis of coseismic and postseismic variations of the Earth's gravity field is carried for the regions of three giant earthquakes (Andaman–Sumatra, December 26, 2004, magnitude $M_w = 9.1$; Maule–Chile, February 27, 2010, $M_w = 8.8$, and Tohoku-Oki, March 11, 2011, $M_w = 9.0$) with the use of GRACE satellite data. Within the resolution of GRACE models, the coseismic changes of gravity caused by these seismic events manifest themselves by large negative anomalies located in the rear of the subduction zone. The real data are compared with the synthetic anomalies calculated from the rupture surface models based on different kinds of ground measurements. It is shown that the difference between the gravity anomalies corresponding to different rupture surface models exceeds the uncertainties of the GRACE data. Therefore, the coseismic gravity anomalies are at least suitable for rejecting part of the models that are equivalent in the ground data. Within the first few months after the Andaman–Sumatra earthquake, a positive gravity anomaly started to grow above the deep trench. This anomaly rapidly captured the area of the back-arc basin and largely compensated the negative coseismic anomaly. The processes of viscoelastic stress relaxation do not fully allow for these rapid changes of gravity. According to the calculations, even with a sufficiently low viscosity of the upper mantle, relaxation only covers about a half of the observed change of the field. In order to explain the remaining temporal variations, we suggested the process of downdip propagation of the coseismic rupture surface. The feasibility of such a process was supported by numerical simulations. The sum of the gravity anomalies caused by this process and the anomaly generated by the processes of viscoelastic relaxation accounts well for the observed changes of the gravity field in the region of the earthquake. The similar postseismic changes of gravity were also detected for the region of the Tohoku-Oki earthquake. Just as in the case discussed above, this earthquake was also followed by a rapid growth of a positive postseismic anomaly, which partially counterbalanced the negative coseismic anomaly. The time variations of the gravity field in the region of the Maule–Chile earthquake differ from the pattern of changes observed in the island arcs described above. The postseismic gravity variations are in this case concentrated in a narrower band above the deep trench and shelf, and they do not spread over the continental territory, where the negative coseismic anomaly is located. These discrepancies reflect the difference in the geodynamical settings of the studied earthquakes.

DOI: 10.1134/S1069351314020062

INTRODUCTION

The study of temporal variations of the gravity field of the Earth has a long history. As early as the middle of the twentieth century, the repeat gravity surveys at specially arranged reference points were conducted in a number of regions of the world. The ground measurements typically cover relatively small areas, and their accuracy has recently attained about a few tens μGal (1 μGal = 10^{-9} Gal = 10^{-9} cm/s^2). Measurements of temporal variations of gravity are also conducted at stationary points, where high accuracy is achieved with the use of superconducting gravimeters.

At present, there are more than thirty such instruments operating in the world; however, these measurements are local and do not provide a sufficiently detailed insight even into the global and, much less so, regional dynamics of the variations of the gravity field.

The situation changed profoundly on March 17, 2002 after the launch of the satellite-based GRACE mission consisting of twin satellites. At present, the orbital height of the satellites is about 437 km, and the distance between them is about 191 km. The high accuracy and high resolution of GRACE measurements, compared to the previous satellites, is achieved due to three specific features. First, GRACE satellites have a significantly lower orbit; second, their orbits are highly accurate, since orbit determination not only relies on ground tracking alone but also involves GNSS-based tracking from GPS and GLONASS satellites, which fly in high orbits. Third, the distance between the twin GRACE satellites is also measured with high precision (within 10 μm), which, to a certain extent, is similar to the gravity gradient measurements along the satellite trajectories. Construction of the new, highly accurate models of the static gravity field of the Earth, including purely satellite-based models and those based on both the satellite and ground measurements, is not the only probable application of GRACE data. These data can also be used for studying the temporal variations of this field. A number of the research centers calculate and publish on Internet the monthly models of the Earth's gravity field in the form of an expansion in spherical harmonics. For example, such models are issued by GeoForschungsZentrum at Potsdam, Germany; Center for Space Research (CSR) of University of Texas at Austin, the United States; Jet Propulsion Laboratory (JPL) managed for NASA by California Institute of Technology (California, United States); and Space Geodesy Research Group (GRGS) of the National Centre for Space Studies (CNES) in France. GRGS/CNES group calculates the models from monthly data with a time shift of ten days, which yields a series of time-averaged ten-day models containing 50 spherical harmonics. The GRACE mission was initially expected to last for five years; however, the satellites have been operating for eleven years so far and it is hoped that they will continue for another two or three years.

The main intent of GRACE mission was to study the dynamics of the ocean and ice sheets, as well as the large-scale water circulation in the continents. These effects cause geoid height variations by a few millimeters on large spatial scales providing the main contribution to the gravity variations registered by GRACE satellites (Dickey et al., 1997; Wahr, Molenaar, and Bryan, 1998). The theoretical estimates (Gross and Chao, 2001; Mikhailov et al., 2004; Sun and Okubo, 2004; Mikhailov et al., 2005) show that the gravity field variations associated with strong earthquakes can also be recognized from the GRACE models. However, such studies have not been planned initially because it could barely be expected that catastrophic earthquakes, which were absent for about 40 years before the GRACE mission, would occur during the planned five-year period of its operation.

In order to demonstrate the possibility of revealing the earthquake-related gravity field variations, we used the rupture surface models for two earthquakes that occurred in 1960 in Chile ($M_w = 9.5$) (hereinafter, the cited estimates of magnitudes are taken from the NEIC USGS catalogue) and in 1964 in Alaska ($M_w = 9.2$) (Mikhailov et al., 2004). It was shown that GRACE models are sufficiently accurate for revealing the coseismic gravity variations caused by strong earthquakes, such as the event in Alaska. We have also demonstrated that among the three different models suggested by Savage and Hastie (1966) for the earthquake in Chile, which equally well fit the ground geodetic data, it is possible to select the correct model of the surface of the rupture. At the same time, it turned out that revealing the linear temporal trend in the gravity field that corresponds to the growth of stresses and strains within the locked asperity of the Alaska subduction zone requires a higher accuracy, which exceeds the accuracy of the monthly GRACE models by an order of magnitude. This result is important for planning future satellite projects on studying the temporal variations of the gravity field.

Later, de Viron et al. (2008) explored the possibility of recognizing coseismic gravity field variations induced by the earthquakes of different magnitudes. These authors applied the series expansion in the empirical orthogonal functions and found that with the existing accuracy of GRACE gravity solutions, the signals from the earthquakes with $M_w = 9$ and $M_w = 8.8$ can be recognized with a probability of above 98% and about 60%, respectively. The probability of revealing the signals from the earthquakes with magnitude $M_w = 8.6$ is 40%; the signals from the earthquakes with $M_w = 8.3$ can be revealed with a probability of at most 33%.

Later, three great earthquakes occurred during the operation interval of the GRACE Twins: the Andaman–Sumatra earthquake with $M_w = 9.1$ on December 26, 2004, the Mauna Chile event with $M_w = 8.8$ on February 27, 2010, and the Tohoku-Oki mega-earthquake with $M_w = 9.0$ on March 11, 2011. These seismic events gave impetus to the extensive research of temporal variations of gravity in the regions of these earthquakes with the use of GRACE gravity models.

In this paper, we explore the possibility of studying the coseismic and postseismic processes by the combined analysis of GRACE gravity solutions and ground data. We present some results of geodynamical modeling aimed at verifying the conclusions suggested by this combined interpretation. We did not intend to explicitly review numerous publications on the subject; therefore, we only refer to few key studies.

THE ANDAMAN–SUMATRA EARTHQUAKE

This earthquake is one of the strongest seismic events that occurred during the last 100 years and the first event that has been investigated by satellite gravimetry. The epicenter of the earthquake is located in the zone where the Indo-Australian Plate submerges beneath the southeastern part of the Eurasian Plate west of the northern tip of Sumatra. The detailed study of the earthquake revealed the complex character of this event. According to the seismological data, within the first 200–220 s, the rupture advanced over a distance of 400 km (the model of C. Li published on the NEIC website (http://earthquake.usgs.gov/regional/neic)). The geodetic data suggest that later, the rupture propagated further northwards by about 900 km, although at a lower velocity and without generating seismic waves (Ammon et al., 2005; Banerjee, Pollitz, and Bürgmann, 2005; Lay et al., 2005; Vigny et al., 2005). This was followed by numerous aftershocks and the Nias earthquake, which occurred on March 28, 2005 and had a magnitude of $M_w = 8.6$.

The coseismic gravity anomaly that emerged due to the earthquake was recognized by many authors. Han et al. (2006) studied gravity variations by analyzing the changes in the distance between the twin satellites. These authors compared the real observed effect with the synthetic anomaly calculated from the rupture surface model in the idealized situation of an elastic halfspace. They considered the effects associated with the displacement of density interfaces and the effects caused by variations in the density of a compressible medium due to the changes in the stress distribution. We note that the latter effect is predominant in the low-order spherical harmonics of GRACE solutions. The authors of the quoted study concluded that the predicted and observed variations of gravity are quite similar, although the data used in the analysis were averaged over six months after the earthquake; i.e., they contained the Nias earthquake of March 28, 2005.

In order to distinguish the temporal variations in the region of the Andaman-Sumatra earthquake against the intense background noise, Panet et al. (2007) applied continuous wavelet transform and averaging on incremental time intervals. In the quoted study, the third-order Poisson multipoles suggested by Holschneider, Chambodut, and Mandea (2003) were used as the spherical wavelet basic functions $\varphi_a^e(\varphi,\lambda)$. These multipoles on the sphere belong to space $L_2(S)$ and are described by the position $a = (\varphi_0, \lambda_0)$ and scale parameter e. If the analyzed function g is also square-integrable on the sphere S of radius R, which is equal to the Earth's radius in our case, then the continuous wavelet transform is determined as a scalar product of these two functions:

$$C^e(a) = (\varphi_a^e(\varphi,\lambda)g(\varphi,\lambda)). \quad (1)$$

The Poisson multipoles have a zero mean on the sphere, therefore the function $C^e(a)$ is proportional to the coefficient of correlation between the given function and the wavelet, depending on its position on the sphere and spatial scale. The wavelet transform can be conducted with different normalizations. The calculations for Sumatra presented below are carried out by formula (1) without normalization. For Japan and Chile, the results of integration by (1) are divided by the L_2-norm of the wavelet. In the first case, the outcome is obtained in arbitrary units; the results obtained in the second case can be assumed to have the same units as gravity field used in the transformation. However, the type of normalization is not important because, when comparing the predicted and real data, all the functions have been subjected to identical transformations.

By calculating wavelet transforms $C^e(a)$ for different positions a and scale e of the wavelet, one can explore the function g for the presence of the components with a wavelength in the vicinity of a given scale e. This analysis is very efficient for isolating weak localized signals against the noise distributed across the sphere.

In order to extract actual gravity variations (Panet et al. (2007) used the models mentioned above (GRGS/CNES). Construction of these models is described in detail by Biancale et al. (2008). By comparing the predicted anomaly with the empirical data on different wavelet scales, we found that the actual anomaly has a slightly higher amplitude than predicted by the rupture surface model (Fig. 1). For explaining this discrepancy, we hypothesized in (Panet et al., 2007) that the overriding plate is heterogeneous in terms of its strain properties; therefore, the extension caused by the earthquake was stronger in the lithosphere of the Andaman Sea, which is broken by the faults. The additional subsidence calculated in the heterogeneous elastic plate model compensated the difference between the calculated and real gravity anomalies.

The previous studies have demonstrated that the resolution and accuracy of GRACE gravity models is sufficient for verifying and elaborating the geodynamical models of coseismic processes based on seismological and geodetic data. We note that the method suggested by Panet et al. (2007) for noise suppression also revealed the gravity anomaly that emerged as a result of the Nias earthquake on March 18, 2005, which had a significantly lower magnitude $M_w = 8.6$.

De Linage et al. (2009) and Broerse et al. (2011) studied the effects of water dynamics on the surface of the planet in their calculations of the synthetic coseismic anomaly. They suggested to introduce isostatic correction for the change in the thickness of the water layer, caused by coseismic displacements of the ocean bottom. In fact, this correction is almost completely composed of the effects caused by the changes in the thickness of the water layer due to the displacement of

the ocean floor. This effect is taken into account automatically if one uses (quite naturally) the density contrast between the Earth's crust and water when calculating the changes of gravity due to the surface displacement beneath the sea level and the density contrast between the crust and air in the calculations for the land regions.

THE POSTSEISMIC CHANGES OF GRAVITY FIELD IN THE REGION OF THE ANDAMAN-SUMATRA EARTHQUAKE

The analysis of the gravity field variations at the postseismic stage (Panet et al., 2007; Ogawa and Heki, 2007; Linage et al., 2009) revealed very fast growth of the gravity anomaly. This anomaly originated at the Sumatra trench and above coseismic rupture and then rapidly expanded northeast so that the main part of the negative coseismic anomaly was compensated, and only a small part of the coseismic minimum persisted above the southern segment of Indo-China Peninsula (Fig. 2). According to the estimates of Panet et al. (2010), the amplitude of the positive anomaly 26 months after the earthquake is, on average for the wavelets of different scales, 70% of the coseismic anomaly. According to de Linage et al. (2009), the amplitude of the postseismic anomaly over this period is almost equal to the amplitude of the coseismic anomaly.

It is important to note that the high rate of postseismic gravity field variations corresponds to the high displacement velocities recorded at the postseismic stage by GNSS GPS (e.g., Vigny et al., 2005). These GPS data were mainly accounted for by the processes of postseismic displacements on the rupture surface and/or on its downdip extension, as well as by viscoelastic stress relaxation. Masterlark et al. (2001) have demonstrated that the poroelasticity process yields too local an effect and does not explain the observed displacements. We also note the study of Ogawa and Heki (2007), who consider water diffusion from the mantle after the earthquake. The relative contributions of these processes cannot be assessed from the GPS data alone. Indeed, the postseismic displacements in the lower part of the coseismic rupture surface fully explain the observed geodetic data (Hashimoto et al., 2006). At the same time, good agreement between the crustal deformations derived from the GPS data and the corresponding predictions is achieved in the model of viscoelastic relaxation in a spherical radially symmetric Earth (Pollitz, Bürgmann, and Banerjee, 2006). For describing the rheology of the asthenosphere, these authors used the biviscous Burgers' body, which has a high viscosity for the steady-state processes and lower viscosity for the short-period transient processes. The best fit of the GPS data is achieved with the following parameters: the thickness of the effective elastic lithosphere is 60 km; the asthenospheric layer occupies the depth interval from 60 to 220 km, its viscosity is 4×10^{17} Pa s in the transient processes and 10^{19} Pa s in the steady-state processes; the upper-mantle layer below the asthenosphere up to a depth of 660 km has a constant viscosity of 10^{19} Pa s.

Panet et al. (2010) applied this model for calculating the temporal variations of the gravity field. For comparison, all the functions were subjected to the wavelet transforms (1). For tracing the evolution of gravity field, we used the GRGS (CNES) models mentioned above (Biancale et al., 2008) for the time interval from August 2002 to September 2007. The models in the form of spherical expansion up to the 50th harmonic are freely accessible at http://grgs.obs-mip.fr/grace/variable-models-grace-lageos/grace-solutions- release- 01#tab2. These models are corrected for gravity effects caused by the circulation of the atmosphere and ocean and by oceanic tides (see details on the cited website). The residual anomalies are mainly contributed by the effects associated with the response to the changes in the volume of continental water and polar ice, the geodynamical effects, and various kinds of noise. The noise typically produces the anomalies that are stretched along the meridian and related to the different sensitivity of the GRACE system to the changes of the field along and perpendicular to the orbit. In order to suppress this effect, the coefficients of spherical harmonics in the GRGS models are determined under the condition that above the 30th harmonic, the coefficients of the harmonic terms decay at the same rate as the coefficients of the static EIGEN-GL04S model (Biancale et al., 2008) based on the GRACE data for the long interval of observations.

Using the wavelet expansions and summation over increasing time intervals, we obtained a stable time series of the changes of the geoid height anomalies without any additional assumptions on the character of their decay (Panet et al., 2010). De Linage et al. (2009) assumed that the coseismic anomaly of the geoid decays exponentially with time. The time-decay constant was estimated at 8.4 months. The approximation of the time series obtained in (Panet et al., 2010) gives the similar time constants (8.0–8.5 months) (Mikhailov et al., 2013).

It is worth noting that the geoid anomaly calculated from the model of viscoelastic relaxation covers up to 80% of the observed decay rate of the geoid anomaly on the small wavelet scales (600 km) and about 60% of it on the large scales (1400 km). These discrepancies are significantly larger than the error of computations; therefore, Panet et al. (2010) suggested considering the postseismic creep on the depth extension of the coseismic rupture surface for explaining the observed discrepancy. It was shown that, for compensating the difference between the synthetic and real anomaly, it is sufficient that a displacement with a total amplitude of about 75 cm occur within 33 months after the earth-

quake on a segment of the plate contact located below the coseismic rupture surface and having an along-dip length of 100 km. A similar suggestion was later offered by Paul et al. (2012), where postseismic displacements with a rate of about 50 cm per year were assumed on the depth extension of the coseismic rupture surface. Hu and Wang (2012) distributed the postseismic displacements both across the surface of the rupture and on its depth extension.

The assumption that postseismic deformations are localized exactly on the downdip continuation of the rupture surface are associated with the fact that a viscoelastic model (Pollitz, Bürgmann, and Banerjee, 2006) well describes the displacements of the Earth's surface recorded by GPS satellites. Therefore, the model of postseismic deformations should not yield a significant effect on the Earth's surface.

In order to verify the hypothesis of postseismic deformations, Mikhailov et al. (2013) carried out numerical simulation of stress accumulation, their release by the earthquake, and subsequent relaxation. The initial conditions were determined by modeling the steady-state subduction with the geometry closely reproducing the structure of the Andaman–Sumatra subduction zone using the I2ELVIS finite-element code (Gerya and Yuen, 2007; Gerya, 2011). The code solves thermo-mechanical equations coupled with petrological processes that take place in the subduction zone. The shorter seismic cycle was modeled with the use of the FLAC (Fast Lagrangian Analysis of Continua) algorithm, where, together with viscoelastic rheology, also the formation conditions of failure zones are introduced, which makes it possible to simulate large deformations associated with the formation of the faults (e.g., (Lyakhovsky, Hamiel, and Ben-Zion, 2011)). Without going deep into the detail of the simulation (whose particularized description and relevant references can be found in (Mikhailov et al., 2013)), we only note the main result here. The results of the simulations show that the stress field that was accumulated during the beginning of the postseismic interval leads to the formation of three failure zones (faults) located on the downdip extension of the coseismic rupture surface (Fig. 3). The down-dip extension of the fault zone was about 100 km, and the cumulative displacement on these faults over 2.5 years attained 1 m. The synthetic gravity field variations have a time-decay coefficient close to the observed value. The total effect of viscoelastic relaxation and postseismic creep completely accounts for the observed evolution of gravity anomaly. It is important that the displacements distributed on the three failure zones (Fig. 3) induce very low slip rates on the surface, which lie at the limit of accuracy of the geodetic measurements.

Thus, the detection of very high rates of the evolution of postseismic processes was one of the main results yielded by the analysis of the ground- and satellite-based data in the region of the Andaman–Sumatra earthquake. The GPS-based postseismic surface deformations and fast growth of the positive gravity anomaly can be interpreted as the joint effect of viscoelastic stress relaxation with the rather low viscosity of the asthenosphere and the postseismic creep on the downdip continuation of the surface of coseismic rupture. It is important that the latter process, which was revealed from satellite gravity data and supported by numerical modeling, cannot be detected with the existing accuracy of the present-day geodetic measurements.

Consider now the recent catastrophic earthquakes in order to compare them with the Andaman-Sumatra event. We start with the Tohoku-Oki mega-earthquake, which occurred in the geodynamical setting similar to that of the earthquake discussed above.

TOHOKU-OKI MEGA-EARTHQUAKE OF MARCH 11, 2011

This catastrophic event had a slightly lower magnitude (9.0–9.1); the horizontal surface displacements reached 10–30 m and a few meters along the vertical (e.g., (Ozawa et al., 2011)). An exceptionally large amount of data has been gained for this earthquake. In particular, these data include the displacements of the Earth surface, ocean bottom, and water level recorded by the seismic stations, stationary GPS points, ocean bottom stations, and tidal gauges. The detailed model of crustal displacement field was suggested by Pollitz, Bürgmann, and Banerjee (2011). These authors note that, since the inversion for the rupture surface geometry and the displacement field on it is not robust, the rupture-surface models for the Tohoku-Oki earthquake derived from different sets of data diverge considerably. For example, the models that are based on the seismic waveforms, either with or without allowance for the GPS data and tsunami waveforms, yield the slip on the rupture surface of up to 50 m, whereas the model of Pollitz, Bürgmann, and Banerjee (2011), which only uses the GPS data, estimates maximal displacements at 33 m. The position of the area of maximal displacement also greatly varies along the dip. Different authors find it occurred downdip of the hypocenter (Ammon et al., 2011; Ozawa et al., 2011; Simons et al., 2011), or slightly updip of the hypocenter (Pollitz, Bürgmann, and Banerjee, 2011; Shao et al., 2011), or at a shallow depth nearby the trench (Lay et al., 2011).

The postseismic displacements, just as the distribution of the aftershocks, suggest southward propagation of the rupture during about a day and a slip of up to 1 m on the rupture surface.

Pollitz, Bürgmann, and Banerjee (2011) note the following features of the displacement field in the region of the Tohoku-Oki event, which are important for the further analysis. Before the earthquake, the northeastern coast of Japan was overall subsiding. This was probably associated with the fact that the segment

Fig. 1. (a) The continuous wavelet transform of the (a, b) predicted and (c) real geoid height variations due to the Andaman-Sumatra earthquake of December 26, 2004. The real temporal variations are calculated as the difference between the GRGS/CNES gravity models for January 2005 and January 2004. The spherical Poisson's multipole with a scale size of 620 km is applied. The scale spans from 0.23 to 0.1 arbitrary units. (a) The synthetic gravity anomaly as a result of the displacement on the rupture surface with the parameters suggested in (Banerjee et al., 2007) was calculated using the model of self-gravitating spherically layered planet (Pollitz, 1996). (b) The same as (a) with the additional subsidence due to the stronger extension of the Andaman Sea lithosphere. (c) The real gravity anomaly retrieved by the continuous wavelet transform (1).

Fig. 2. The evolution of the geoid anomaly after the Andaman–Sumatra earthquake. The map in the upped left shows the coseismic anomaly (the difference between the gravity field in January 2005 and January 2004), which has been subjected to the wavelet transform (1) with the Poisson's multipole with a scale size of 1200 km. Then this anomaly has been subtracted in order to demonstrate the growth of the positive anomaly with time. Index n denotes the number of the months after the earthquake. In order to suppress the oscillations in the course of time, the postseismic anomalies are averaged over the incremental time intervals. For example, the postseismic anomaly with index n is the sum of the anomalies from the 1st to the nth month divided to n.

of the subduction zone, which was completely locked, extended to a depth of 60 km, while the partially locked area could have reached a depth of 100 km. Since in the Late Quaternary, this region overall was rising, we may quite reasonably expect that interseismic submergence was compensated by coseismic uplifting. However, the Tohoku-Oki event was accompanied by the subsidence of the coastal area. In order to provide this, the rupture should not extend below a depth of 35 km. This combination of the movements is characteristic of the strong subduction earthquakes, which are often followed by a fast downdip expansion of coseismic rupture (Heki, 2007). In the quoted paper, Heki presents the example of the Miyagi-Oki earthquake of 1978, which had a magnitude of 7.4. This event was accompanied by weak coseismic subsidense of the coastal area. Instead of the ongoing subsidence, the postseismic uplift probably due to the postseismic creep beneath the surface of a coseismic rupture was observed. Considering this, Pollitz, Bürgmann, and Banerjee (2011) discussed the problem of how deep had the locked segment of the contact between the lithospheric plates propagated in the region of the Tohoku-Oki earthquake? We made an attempt to answer this question by analyzing the variations of gravity field during and after the earthquake in the similar way we have done for the Andaman-Sumatra earthquake. The temporal variations of gravity in the region of the earthquake were studied with the use of the models provided by Center for Space Research (CSR) of the University of Texas at Austin, United States. The models are provided in the form of spherical expansion of up to the 60th spherical harmonic.

The coseismic gravity variations on four wavelet scales are shown in Fig. 4. Just as in the region of Sumatra, this anomaly in the first 60 harmonics of spherical expansion of the gravity field appears as a vast area of negative values in the back-arc of the subduction zone above the Sea of Japan and the quite small area of positive values in the region of the trench. Figure 4 shows the anomaly that has been formed by June 2011, i.e., three months after the earthquake. After the earthquake, the geoid anomaly continued to increase probably due to the postseismic creep both on the surface of the seismic rupture and on its southern extension. Using the GRACE data, Wang et al. (2012) constructed the model of the rupture surface and estimated moment for the total slip on the coseismic and postseismic (up to June 2011) intervals at 4.6×10^{22} N m. They also calculated the moment for a number of rupture surface models based on purely seismic or seismic plus geodetic data. The average moment over three different models was estimated at 3.8×10^{22} N m. According to Wang et al. (2011), this increase in the

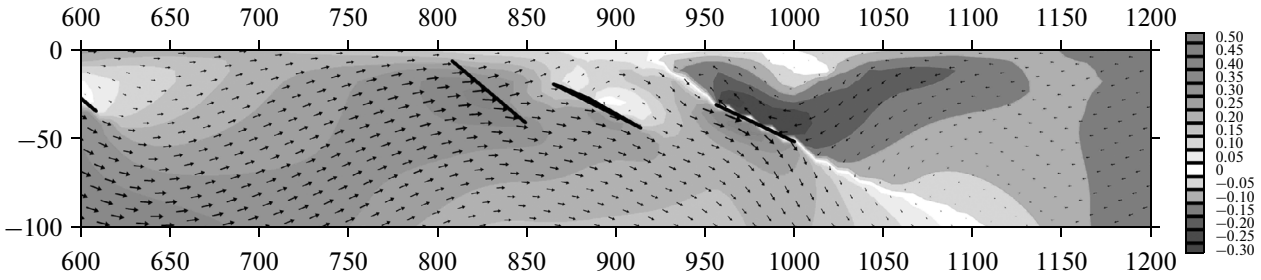

Fig. 3. The synthetic postseismic displacement field (in m) in the model of the subduction zone 36 months after the seismic event. The amplitude of the displacements is shown by the grades of shading, and the direction of the displacements is shown by the arrows. The maximal size of the arrow corresponds to the displacement of 0.62 m. The black lines delineate the failure areas. The inclined zone of zero displacements running through the right fault zone coincides with the top of the submerging plate.

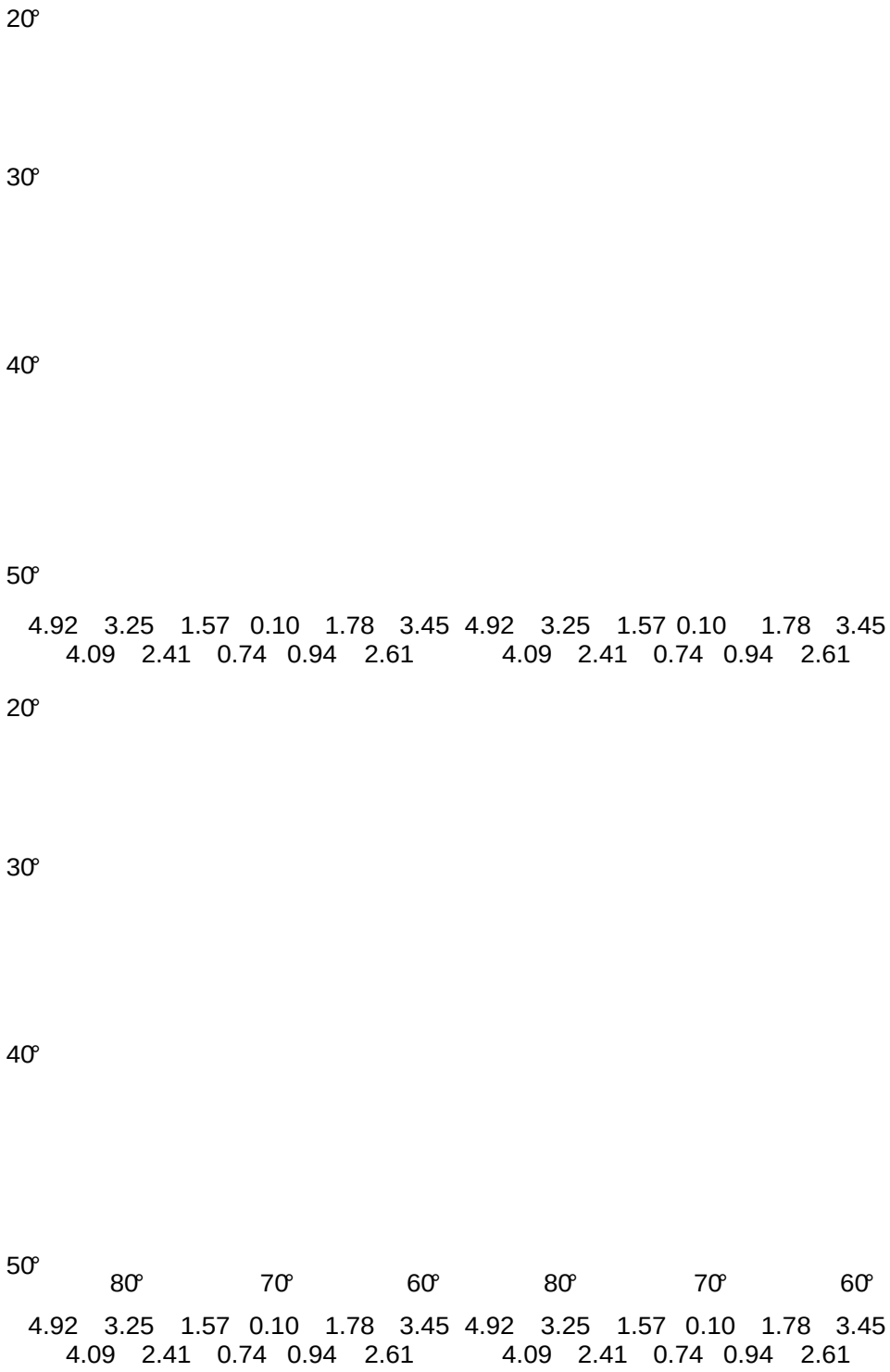

Fig. 8. The coseismic geoid height anomaly for the region of the Maule Chile earthquake of February 27, 2010 calculated for different wavelet scales. The upper line of the graphs corresponds to the scale sizes of 1200 and 1000 km; the lower line of the graphs corresponds to the scales of 800 and 600 km.

This averaging suppresses the amplitude of the short term signals and leaves unaffected the rate of the exponential decay (if any). The dashed line depicts the exponential decay

$$C + Ae^{t/B}, \quad (3)$$

calculated for the postseismic interval from the condition of the best fit in the sense of root mean squares. It

can be seen in Fig. 7 that the exponential decay is clearly pronounced on the large wavelet scales and is less distinct on the scale of 600 km, which could probably be due to the higher noise level on the short wavelengths.

The time series are strongly contaminated with noise, therefore approximation (3) is unsuitable for a robust estimate of the time-decay constant B. Within widely varying B, the root mean square error of approximation changes insignificantly. At the same time, parameters C and A are determined robustly, particularly on the large wavelet scales. In a wide interval of the time-decay constant, the amplitude of relaxation A makes up about 50% of the coseismic jump in the geoid heights ($C + A$) on the wavelet scale of 1200 km and about 40% on the scale of 1000 km, which is close to the estimates presented in (Panet et al., 2010) for the Andaman-Sumatra earthquake region. The preliminary results of modeling the viscoelastic relaxation show that one year after the earthquake, the amplitude of the induced gravity anomaly reached about 50% of the coseismic anomaly (F. Pollitz, personal communication).

Thus, the analysis of gravity models shows that variations in the geoid heights during and after the Tohoku-Oki earthquake are similar to those detected in the region of the Andaman–Sumatra seismic event. These results, together with the conclusions based on the analysis of geodetic data (Polliz et al., 2011), support the hypothesis of the postseismic downdip propagation of the surface of seismic rupture in this region as well. Consider now the Maule earthquake in Chile, which occurred in a quite different geodynamical setting.

THE MAULE–CHILE EARTHQUAKE ON FEBRUARY 27, 2010

This seismic event had a magnitude of $M_w = 8.8$ and, just as the events discussed above, it was also recorded by the GRACE satellites (e.g., (Wang et al., 2012)). Here again, similar to the analysis of the Tohoku-Oki earthquake, we used the models developed in the Center for Space Research of the University of Texas at Austin, United States, for studying the temporal gravity variations. As has been mentioned above, these models contain 60 spherical harmonics. Figure 8 displays the coseismic changes of gravity revealed for four different wavelet scales.

The synthetic coseismic geoid variations shown in Fig. 9 are calculated from the rupture surface model constructed in (Lorito et al., 2011). The model is composed of 200 elements distributed in 25 lines along the strike and 8 columns along the dip in accordance with the geometry of the subducting slab. The elements are 25 × 25 km in size and the bottom boundary of the model is located at a depth of 63 km. The direction and amplitude of the displacements are found by the inversion of the geodetic data and tsunami waveforms.

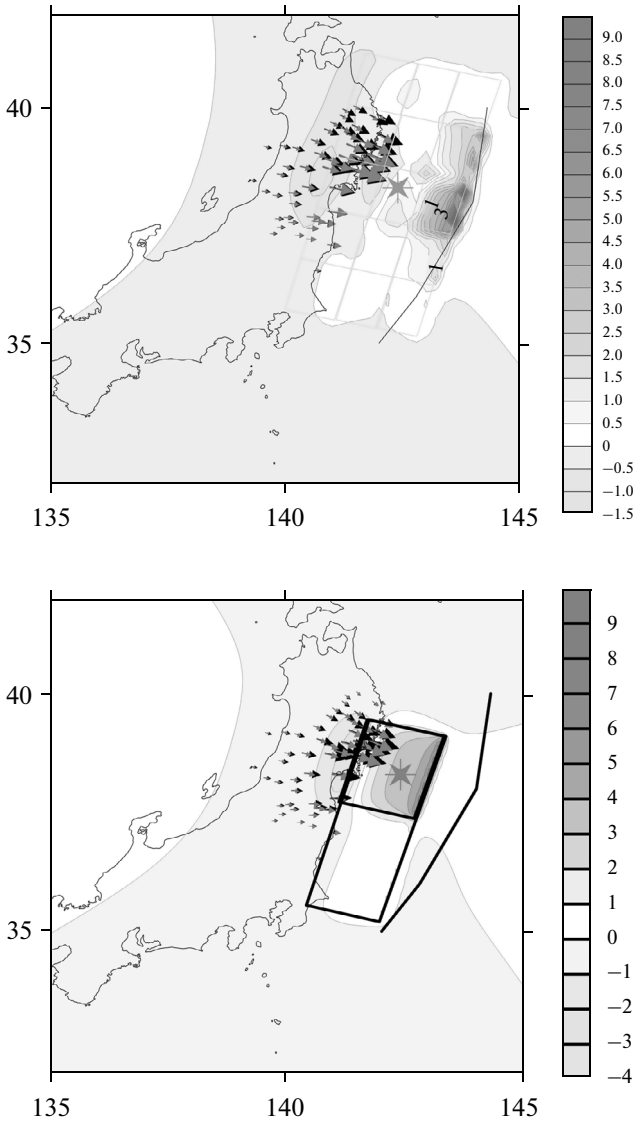

Fig. 5. The displacements (in m) on the Earth's surface calculated from the rupture surface models of K. Hayes (http://earthquake.usgs.gov/earthquakes/eqinthenews/2011/usc0001xgp/finite_fault.php). The rupture area in the model composed of 325 elements is contoured by squares in the upper panel. In order to avoid overloading the figure, the elements are amalgamated in groups of five elements along the strike and 3–4 elements along the dip. In the lower model, the rupture surface includes two elements. The black and gray arrows correspond to the actual GPS-based and calculated horizontal displacements. The broken line shows the approximate position of the deep oceanic trench. The grayscale bar shows the amplitude of vertical displacements on the Earth's surface in m. The position of the epicenter is marked by the asterisk.

The amplitudes of the displacements are strongly depth-specific. The largest displacements are localized in the middle part of the plate contact where they attain 18.5 m; at a depth below 45 km, the displacements measure 1–2 m.

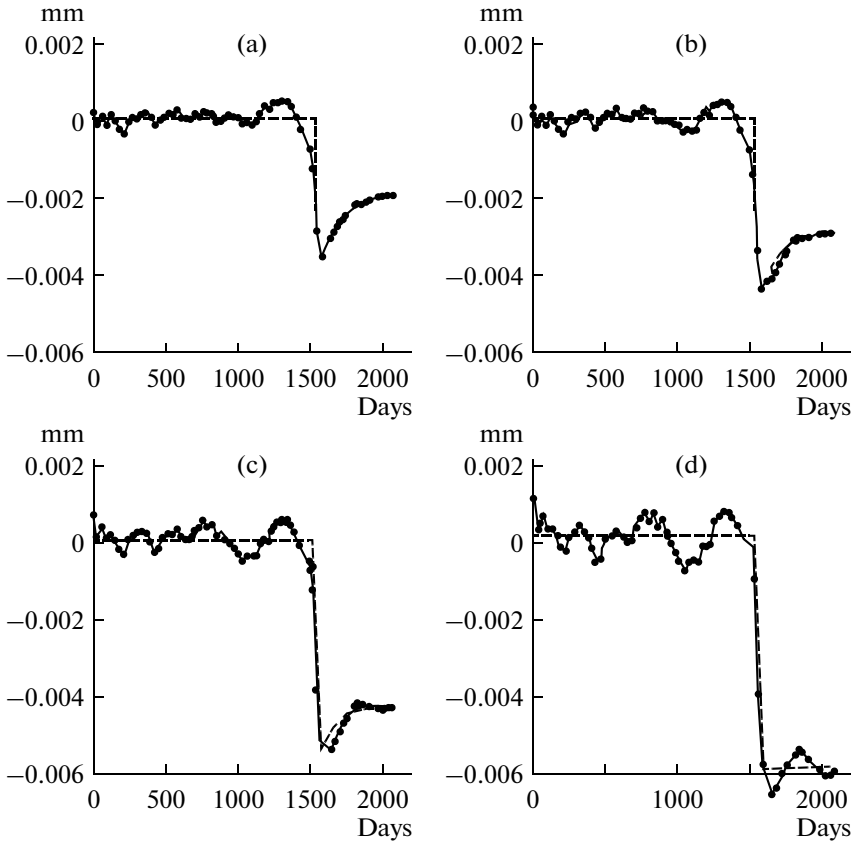

Fig. 7. The time series of the variations in the wavelet coefficients on four scales in the region of the Tohoku-Oki earthquake. The scale sizes of the wavelet are (a) 1200 km, (b) 1000 km, (c) 800 km, and (d) 600 km.

Although the anomaly in Chile is significantly weaker than in the regions of Sumatra and Japan, the gravity models still have sufficiently high resolution to allow tracing the postseismic evolution of gravity field, which, just as in the other cases, consists in the growth of a positive anomaly. This anomaly is formed above the oceanic trench; however, in this case, it is not shifted towards the overriding plate and it does not capture the zone of negative coseismic anomaly. The time series of the geoid variations in the epicenter of the coseismic geoid anomaly, on the margin of this anomaly and outside it (where the coseismic deformations are close to zero) are shown in Fig. 10. It can be seen that the postseismic changes with an amplitude of up to 1 mm occur above the trench (point 3) and shelf (point 2), whereas the variations at the epicenter of the coseismic anomaly are significantly lower (point 1).

This change of gravity pattern after the earthquake probably indicates that the postseismic creep at large depths does not occur in this geodynamical setting.

Comparison of the amplitude of coseismic negative anomaly of the geoid (in mm) with the theoretical predictions by the first and second models of G. Hayes (USGS) for the spherical wavelet scales of 600, 800, 1000, and 1200 km

	600 km	800 km	1000 km	1200 km
Model of 2 elements	−5.0	−4.2	−3.5	−2.9
Model of 325 elements	−8.8	−7.8	−6.6	−5.7
Actual changes in the geoid heights during the interval from the 121st to 151st days of 2011	−5.9	−5.2	−4.3	−3.5

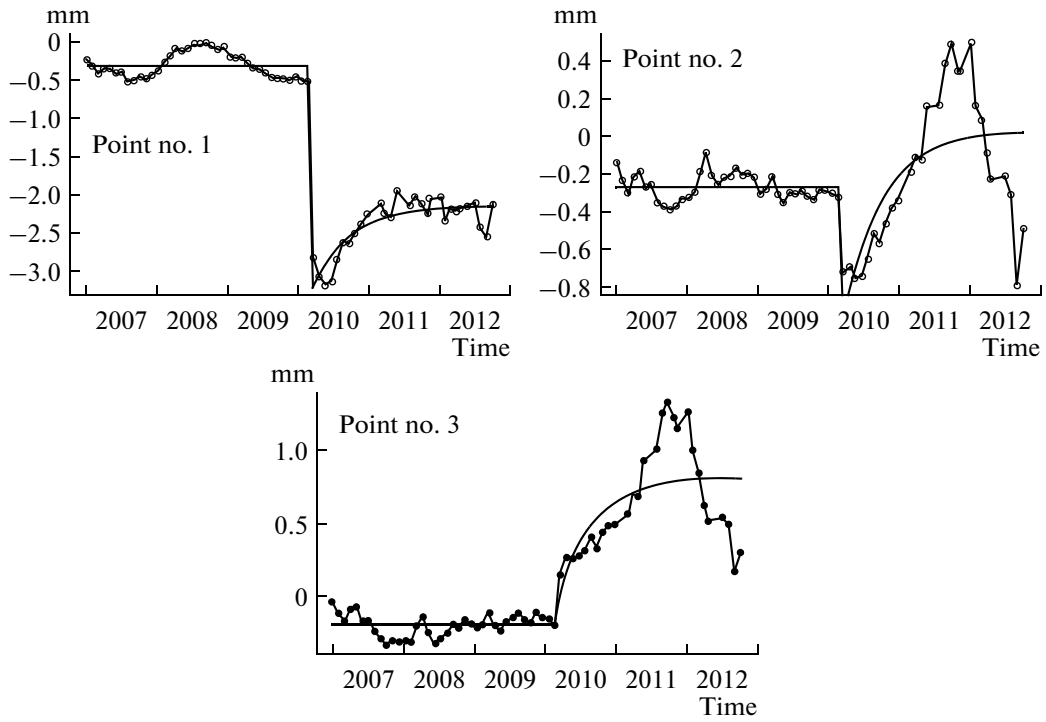

Fig. 10. The postseismic evolution of the geoid anomaly in the region of the Maule–Chile earthquake of 2010 calculated with the use of spherical wavelets of scale 1000 km at three points shown in Fig. 9. The horizontal axis is time, and the vertical axis shows mm of the geoid (note that the scales are different).

The postseismic displacements below the Moho in the case of the Andaman–Sumatra earthquake were estimated at about 1 m. In the case of the earthquake in Chile, this amount of displacement is achieved in the model of the coseismic displacement. The process of viscoelastic relaxation after the earthquake in the ocean–ocean subduction zone can occur in a different way than in the subduction zone of the oceanic plate beneath the continental plate.

CONCLUSIONS

Our study shows that the analysis of temporal variations of gravity in the regions of strong earthquakes yields new information, which adds considerably to the information retrieved from the ground measurements. The coseismic gravity changes generally agree with the theoretically predicted variations calculated from the models of seismic rupture. We note that the problem of reconstructing the displacements on the rupture surface is unstable, and the results of the inversions considerably differ depending on the amount of the initial data, the resolution of the model, and the method of solution. The discrepancies between the gravity field variations calculated from different models are noticeably higher than the errors of GRACE gravity models; therefore, the gravity data can be used at least for sorting out the models of the rupture surface.

The postseismic variations of the Earth's gravity field carry the information about the processes in the upper mantle of the Earth, which are poorly detectable by the ground methods. These changes in the region of the Andaman–Sumatra earthquake include nucleation of the positive anomaly of the geoid above the oceanic trench and rapid expansion of this anomaly over the entire region occupied by the coseismic negative anomaly. As a result, the amplitude of the coseismic anomaly drops to 70% and even stronger during 25–30 months after the seismic event. In order to explain the observed temporal variations of gravity in the region of Sumatra, we suggest the model of postseismic creep on the downdip continuation of the coseismic rupture. The numerical modeling has supported this model.

Similar postearthquake changes of gravity have also been detected in the region of the Tohoku-Oki earthquake, where the positive postseismic anomaly has also grown and partially compensated the negative coseismic anomaly. The temporal variations of the gravitaty field in the region of Maule–Chile earthquake differ to some extent from the changes recorded in the ocean–ocean subduction zones considered above. The postseismic changes of gravity are localized in a narrower band above the trench; they do not capture the area of the negative coseismic anomaly. This character of the changes of the gravity field can probably indicate that the rupture in Chile has immediately ripped deep down, and significant postseismic creep at

a large depth did not occur. Apparently, these discrepancies reflect the significant difference in the geodynamical settings that gave rise to the discussed seismic events.

ACKNOWLEDGMENTS

The work was supported by the Russian Foundation for Basic Research (RFBR) grant no. 12-05-00276. The joint research by Russian and French authors was partly supported by the CNRS-RFBR grant no. 12-05-91051.

REFERENCES

Ammon, C., Ji, C., Thio, H.-K., Robinson, D., Ni, S., Hjorleifsdottir, V., Kanamori, H., Lay, T., Das, S., Helmberger, D., Ichinose, G., Polet, J., and Wald, D., Rupture process of the 2004 Sumatra-Andaman earthquake, *Science*, 2005, vol. 308, pp. 1133–1139.

Ammon, C.J., Lay, T., Kanamori, H., and Cleveland, M. A rupture model of the 2011 off the Pacific coast of Tohoku earthquake, *Earth Planets Space*, 2011, vol. 63, pp. 693–696. doi: 10.5047/eps.2011.05.015

Banerjee, P., Pollitz, F., and Bürgmann, R., Size and duration of the great 2004 Sumatra-Andaman earthquake from far-field static offsets, *Science*, 2005, vol. 308, pp. 1769–1772.

Banerjee, P., Pollitz, F., Nagarajan, B., and Burgmann, R., Coseismic slip distribution of the 26 December 2004 Sumatra-Andaman and 28 March 2005 Nias earthquakes from GPS static offsets, *Bull. Seismol. Soc. Am.*, 2007, vol. 97, no. 1A, S86–S102.

Biancale, R., Lemoine, J.M., Balmino, G., Bruinsma, S., Perosanz, F., Marty, J.C., Loyer, S., Bourgogne, S., and Gégout, P., 6 years of gravity variations from GRACE and LAGEOS data at 10-day intervals over the period from July 29th 2002 to November 13th, 2008. http://bgi.cnes fr:8110/geoid-variations/README.html (2009)

Broerse, D.B.T., Vermeersen, L.L.A., Riva, R.E.M., and van der Wal, W., Ocean contribution to co-seismic crustal deformation and geoid anomalies: application to the 2004 December 26 Sumatra–Andaman earthquake, *Earth Planet. Sci. Lett.*, 2011, vol. 305, pp. 341–349.

Cambiotti, G. and Sabadini, R., Source model for the great 2011 Tohoku earthquake (M_w = 9.1) from inversion of GRACE gravity data, *Earth Planet. Sci. Lett.*, 2012, vols. 335–336, pp. 72–79.

Dickey, J.O., Bentley, Ch.R., Bilham, R., Carton, J.A., Eanes, R.J., Herring, Th.A., Kaula, W.M., Lagerloef, G.S.E., Rojstaczer, S., Smithg, W.H.F., van den Dool, H.M., Wahr, J.M., and Zuber, M.T., *Satellite Gravity and the Geosphere*, Washington: Natl. Academy Press, 1997.

Gerya, T.V. and Yuen, D., Robust characteristics method for modeling multiphase visco-elasto-plastic thermomechanical problems, *Phys. Earth Planet. Inter.*, 2007, vol. 163, pp. 83–105.

Gerya, T.V., Future directions in subduction modelling, *J. Geodynam.*, 2011, vol. 52, pp. 344–378.

Gross, R. and Chao, B., The gravitational signature of earthquakes, in *Gravity, Geoid and Geodynamics 2000. IAG symposia*, New York: Springer, 2001, vol. 123, pp. 205–210.

Han, S.-C., Shum, C.K., Bevis, M., Ji, C., and Kuo, C.-Y., Crustal dilatation observed by GRACE after the 2004 Sumatra-Andaman earthquake, *Science*, 2006, vol. 313, pp. 658–662.

Hashimoto, M., Choosakul, N., Hashizume, M., Takemoto, S., Takiguchi, H., Fukuda, Y., and Frjimori, K., Crustal deformations associated with the great Sumatra-Andaman earthquake deduced from continuous GPS observation, *Earth Planets Space*, 2006, vol. 58, pp. 127–139.

Heki, K., Secular, transient, and seasonal crustal movements in Japan from a dense GPS array: Implication for plate dynamics in convergent boundaries, in: *The Seismogenic Zone of Subduction Thrust Faults*, Dixon, T. and Moore, C., New York: Columbia University Press, 2007, pp. 512–539.

Holschneider, M., Chambodut, A., and Mandea, M., From global to regional analysis of the magnetic field on the sphere using wavelet frames, *Phys. Earth Plan. Int.*, 2003, vol. 135, pp. 107–124.

Hu, Y. and Wang, K., Spherical-earth finite element model of short-term postseismic deformation following the 2004 Sumatra earthquake, *J. Geophys. Res.*, 2012, vol. 117, p. B05404. doi: 10.1029/2012JB009153

Lay, T., Kanamori, H., Ammon, C., Nettles, M., Ward, S., Aster, R., Beck, S., Bilek, S., Brudzinski, M., Butler, R., DeShon, H., Ekström, G., Satake, K., and Sipkin, S., The great Sumatra-Andaman earthquake of 26 December 2004, *Science*, 2005, vol. 308, pp. 1127–1133.

Lay, T., Ammon, C.J., Kanamori, H., Xue, L., and Kim, M., Possible large near-trench slip during the 2011 M_w 9.0 off the Pacific coast of Tohoku earthquake, *Earth Planets Space*, 2011, vol. 63, pp. 687–692.

de Linage, C., Rivera, L., Hinderer, J., Boy, J.-P., Rogister, Y., Lambotte, S., and Biancale, R., Separation of coseismic and postseismic gravity changes for the 2004 Ssumatra-Andaman earthquake from 4.6 yr of GRACE observations and modeling of the coseismic change by normal-modes summation, *Geophys. J. Int.*, 2009, vol. 176, no. 3, pp. 695–714. doi: 10.1111/j.1365-246X.2008.04025.x

Lorito, S., Romano, F., Atzori, S., Tong, X., Avallone, A., McCloskey, J., Cocco, M., Boschi, E., and Piatanesi, A., Limited overlap between the seismic gap and coseismic slip of the great 2010 Chile earthquake, *Nature Geosci.*, 2011, vol. 4, pp. 173–177. doi: 10.1038/NGEO1073

Lyakhovsky, V., Hamiel, Y., and Ben-Zion, Y., A non-local visco-elastic damage model and dynamic fracturing, *J. Mech. Phys. Solids*, 2011, vol. 59, pp. 1752–1776. doi: 10.1016/j.jmps.2011.05.016

Masterlark, T., DeMets, C., Wang, H., Sanchez, O., and Stock, J., Homogeneous versus heterogeneous subduction zone models: Coseismic and post-seismic deformation, *Geophys. Res. Lett.*, 2001, vol. 28, pp. 4047–4050.

Matsuo, K. and Heki, K., Coseismic gravity changes of the 2011 Tohoku-Oki earthquake from satellite gravimetry, *Geophys. Res. Lett.*, 2011, vol. 38, L00G12. doi: 10.1029/2011GL049018

Mikhailov, V., Tikhotsky, S., Diament, M., Panet, I., and Ballu, V., Can tectonic processes be recovered from new gravity satellite data?, *Earth Planet. Sci. Lett.*, 2004, vol. 228, nos. 3–4, pp. 281–297.

Mikhailov, V.O., Tikhotskii, S.A., Diament, M., and Panet, I., Gravity variations of geodynamic origin: recognition and study on the basis of modern satellite gravity data, *Izv., Phys. Solid Earth*, 2005, vol. 41, no. 3, pp. 193–205.

Mikhailov, V., Lyakhovsky, V., Panet, I., van Dinther, Y., Diament, M., Gerya, T., and Timoshkina, E., Numerical modeling of post-seismic rupture propagation after the Sumatra 26.12. 2004 earthquake constrained by GRACE gravity data, *Geophys. J. Int.*, vol. 194, no 2, pp. 640–650. 2013. doi: 10.1093/gji/ggt145

Ogawa, R. and Heki, K., Slow post-seismic recovery of geoid depression formed by the 2004 Sumatra-Andaman earthquake by mantle water diffusion, *Geophys. Res. Lett.*, 2007, vol. 34, p. L06313. doi: 10.1029/2007GL029340

Ozawa, S., Nishimura, T., Suito, H., Kobayashi, T., Tobita, M., and Imakiire, T., Coseismic and postseismic slip of the 2011 magnitude-9 Tohoku-Oki earthquake, *Nature*, 2011, vol. 475, pp. 373–376. doi: 10.1038/nature10227

Panet, I., Mikhailov, V., Diament, M., Pollitz, F., King, G., de Viron, O., Holschneider, M., Biancale, R., and Lemoine, J.-M., Co-seismic and post-seismic signatures of the Sumatra December 2004 and March 2005 earthquakes in GRACE satellite gravity, *Geophys. J. Int.*, 2007, vol. 171, pp. 177–190. doi: 10.1111/j.1365-246X.2007.03525.x

Panet, I., Pollitz, F., Mikhailov, V., Diament, M., Banerjee, P., and Grijalva, K., Upper mantle rheology from GRACE and GPS post-seismic deformations after the 2004 Sumatra-Andaman earthquake, *Geochem. Geophys. Geosys.*, 2010, vol. 11, no 6, Q06008. doi: 10.1029/2009GC002905

Paul, J., Rajendran, C.P., Lowry, A.R., Andrade, V., and Rajendran, K., Andaman postseismic deformation observations: still slipping after all these years?, *Bull. Seismol. Soc. Am.*, 2012, vol. 102, no. 1, pp. 343–351. doi: 10.1785/0120110074

Pollitz, F., Co-seismic deformation from earthquake faulting on a layered spherical Earth, *Geophys. J. Int.*, 1996, vol. 125, pp. 1–14.

Pollitz, F.F., Bürgmann, R., and Banerjee, P., Postseismic relaxation following the great 2004 Sumatra-Andaman earthquake on a compressible self-gravitating Earth, *Geophys. J. Int.*, 2006, vol. 167, pp. 397–420. doi: 10.1111/j.1365-246X.2006.03018.x

Pollitz, F., Bürgmann, R., and Banerjee, P., Geodetic slip model of the 2011 M9.0 Tohoku earthquake, *Geophys. Res. Lett.*, 2011, vol. 38, L00G08. doi: 10.1029/2011GL048632

Savage, J.C. and Hastie, L.M., Surface deformation associated with dip-slip faulting, *J. Geophys. Res.*, 1966, vol. 71, pp. 4897–4904.

Shao, G., Li, X., Ji, C., and Maeda, T., Focal mechanism and slip history of 2011 M_w 9.1 off the Pacific coast of Tohoku earthquake, constrained with teleseismic body and surface waves, *Earth Planets Space*, 2011, vol. 63, pp. 559–564. doi: 10.5047/eps.2011.06.028

Simons, M., Minson, S.E., Sladen, A., Ortega, F., Jiang, J., Owen, S.E., Meng, L., Ampuero, J.-P., Wei, Sh., Chu, R., Helmberger, D.V., Kanamori, H., Hetland, E., Moore, A.W., and Webb, F.H., The 2011 magnitude 9.0 Tohoku-Oki earthquake: Mosaicking the megathrust from seconds to centuries, *Science*, 2011, vol. 332, no. 6036, pp. 1421–1425. doi: 10.1126/science.1206731

Sun, W. and Okubo, S., Coseismic deformations detectable by satellite gravity missions: A case study of Alaska (1964, 2002) and Hokkaido (2003) earthquakes in the spectral domain, *J. Geophys. Res.*, 2004, vol. 109, p. B04405.

Vigny, C., Simons, W., Abu, S., Bamphenyu, R., Satirapod, C., Choosakul, N., Subarya, C., Socquet, A., Omar, K., Abidin, H., and Ambrosius, B., Insights into the 2004 Sumatra–Andaman earthquake from GPS measurements in Southeast Asia, *Nature*, 2005, vol. 436, pp. 201–206.

de Viron, O., Panet, I., Mikhailov, V., Van Camp, M., and Diament, M., Retrieving earthquake signature in GRACE data, *Geophys. J. Int.*, 2008. vol. 174, pp. 14–20. doi: 10.1111/j.1365-246X.2008.03807.x

Wahr, J., Molenaar, M., and Bryan, F., Time variability of the Earth's gravity field: Hydrological and oceanic effects and their possible detection using GRACE, *J. Geophys. Res.*, 1998, vol. 103, pp. 30205–30229.

Wang, L., Shum, C.K., Simons, F.J., Tassara, A., Erkan, K., Jekeli, C., Braun, A., Kuo, C., Lee, H., and Yuan, D.-N., Coseismic slip of the 2010 Mw8.8 Great Maule Chile earthquake quantified by the inversion of GRACE observations, *Earth Planet. Sci. Lett.*, 2012, vol. 335–336, pp. 167–179.

Wang, L., Shum, C.K., Simons, F.J., Tapley, B., and Dai, Ch., Coseismic and postseismic deformation of the 2011 Tohoku-Oki earthquake constrained by GRACE gravimetry, *Geophys. Res. Lett.*, 2012, vol. 39, L07301. doi: 10.1029/2012GL051104

Translated by M. Nazarenko